Salts and Cocrystals of Benzocaine with Increased Dissolution Rate and Permeability Open New Avenues for Enhancing the Duration of Action

CRYSTAL GROWTH & DESIGN

pubs.acs.org/crystal

Article

Salts and Cocrystals of Benzocaine with Increased Dissolution Rate and Permeability Open New Avenues for Enhancing the Duration of Action

Laura Baraldi, Irene Bassanetti, Francesco Amadei, Alessia Bacchi, and Luciano Marchiò*

Cite This: https://doi.org/10.1021/acs.cgd.3c01488

Read Online

ACCESS | Metrics & More | Article Recommendations | Supporting Information

ABSTRACT: Benzocaine, a widely used local anesthetic, has some usage limitations due to its short duration of action, resulting in inconsistent clinical outcomes. In this study, the formation of salts and cocrystals is explored as a strategy to enhance the pharmacokinetic profile of benzocaine, aiming for a higher dissolution rate and permeability in vitro as well as to potentially increase its pharmacological effect and duration of action in vivo. A new cocrystal and nine new salts with two different categories of acids (carboxylic and sulfonic) were prepared and characterized: BH oxalate, BH naphthalenesulfonate, BH camphorsulfonate, BH maleate, BH mesylate, BH tartrate, BH benzenesulfonate, BH *p*-toluenesulfonate, BH esylate (BH: protonated benzocaine), and benzocaine−ligustrazine (cocrystal). Dissolution rate and permeability were improved for all newly synthesized forms. Indeed, every system was completely dissolved within 1 h, while benzocaine was dissolved at 54%, and it was still present in suspension after 4 h. Furthermore, permeability was increased 2-fold for benzocaine maleate and up to seven times for benzocaine camphorsulfonate, highlighting the potential of salification and cocrystallization to increase the in vivo performances of benzocaine.

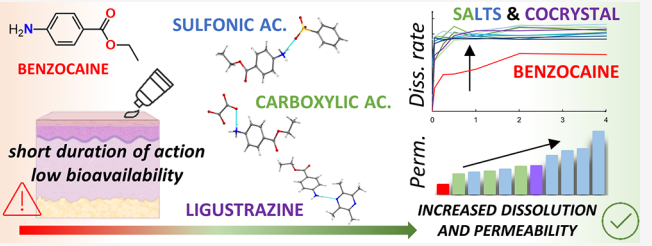

INTRODUCTION

Benzocaine is a widely utilized local anesthetic compound. It is employed for its numbing properties, providing temporary relief from pain and discomfort.[1] Benzocaine acts by inhibiting the transmission of nerve signals in the vicinity of its application, effectively desensitizing the area.[2] However, due to its rapid metabolism and elimination from the body, the anesthetic effect of benzocaine is short-lived. This poses a significant hurdle when aiming for a long-lasting anesthetic effect, especially in cases where prolonged pain relief is desired.[3] In attempts to overcome these pharmacokinetic challenges, researchers have explored various formulation strategies such as nanoencapsulation[4−6] or the use of permeation enhancers to facilitate drug delivery and increase absorption.[7] Furthermore, the development of sustained-release bioadhesive gels has been investigated to prolong the duration of benzocaine's anesthetic effect. These formulations aim to provide a controlled release of the drug over an extended period, reducing the need for frequent administration and enhancing patient compliance. However, these formulations of benzocaine face additional problems: the release dose is often unknown since both the area of contact and the time of contact between the formulation and the skin are not controlled.[8] Moreover, the selection of suitable excipients and the determination of their compatibility with benzocaine is critical to maintain stability and ensure desired release characteristics. The potential for drug-excipient interactions, such as physical or chemical incompatibilities, must be carefully evaluated during formulation development.[9] Additionally, polymorphism, the ability of benzocaine to exist in different crystal forms, can further complicate its pharmacokinetic behavior.[10] Different polymorphic forms may exhibit variations in solubility, dissolution rate, and other physicochemical properties, leading to discrepancies in drug performance.[11,12] Therefore, rigorous characterization and understanding of the specific polymorphic form employed in pharmaceutical formulations are required.

Formulation development studies go beyond the scope of this research; however, our objective is to streamline the process development of the formulation to achieve comparable results by modifying the physicochemical properties of the drug. This aligns with the principle of crystal engineering, which involves the formation of salts and cocrystals, aiming to address challenges such as the pharmacokinetics issues associated with benzocaine.[13,14] The conversion of the drug into a salt or a cocrystal by pairing it with an appropriate counterion or coformer could significantly improve its in vivo

Received: December 14, 2023
Revised: February 9, 2024
Accepted: February 9, 2024

absorption. Indeed, by carefully selecting a molecular counterpart, the resulting system might exhibit enhanced dissolution and permeability properties, leading to improved and lasting pharmacological effect due to the greater amount of drug in the active site and ultimately leading to improved therapeutic outcomes.[15] Enhancing the dissolution rate of benzocaine in a water-based medium could allow a higher loading of the drug in the same time frame, simplifying the formulation development of the drug product.

In the literature, only a few benzocaine salts are reported: benzocaine hydrochloride,[16] benzocaine picrate,[17] benzocaine 3,5-dinitrosalicylate,[18] and benzocaine bis-p-nitrophenylphosphate,[19] even though their pharmacokinetic profile has never been studied. In this work, to investigate the influence of the counterpart on the physicochemical properties of the active compound, two different categories of acids were selected yielding two different groups of salts. The first category includes salts with carboxylic acids: BH oxalate (BO), BH maleate (BMA), and BH tartrate (BT). The second category comprises salts obtained with sulfonic acids: BH naphthalenesulfonate (BN), BH camphorsulfonate (BC), BH mesylate (BME), BH benzenesulfonate (BB), BH *p*-toluenesulfonate (BTS), BH esylate (BE), and BH protonated benzocaine cation. Moreover, we also report the characterization of the benzocaine−ligustrazine (BL) cocrystal. All salts had an increased dissolution rate and a complete dissolution with respect to benzocaine alone. At the same time, they showed a significant enhancement in permeability. The increased dissolution and permeability of the adducts, when compared to benzocaine alone, would potentially lead to a better in vivo performance.

MATERIALS AND METHODS

Benzocaine, maleic acid, methanesulfonic acid, oxalic acid, ethanesulfonic acid, L-(+)-tartaric acid, ligustrazine, 2-naphthalenesulfonic acid, benzenesulfonic acid, *p*-toluenesulfonic acid, (1*S*)-(+)-camphorsulfonic acid, phosphate-buffered saline (PBS) tablets, ethanol 96% (EtOH 96%), acetone, acetonitrile (ACN), and water were used as received from MERCK-Sigma-Aldrich (Taufkirchen, Germany, EU). Solvents were commercially available and used without any other purification. Permeapad barrier used for permeability studies was purchased from innoME GmbH (Espelkamp, Germany).

Salt and Cocrystal Preparations. BO, BN, and BC were synthesized through a classic slurry crystallization method: benzocaine and the acids were suspended in a 1:1 molar ratio into 4 mL of EtOH 96% at room temperature in a 10 mL closed vial and the formation of solid precipitate occurred overnight via slurry. BMA, BH mesylate (BME), and BT were obtained through a slow evaporation crystallization method. Benzocaine and the acids were suspended in a 1:1 molar ratio into 4 mL of EtOH 96% at room temperature in a 10 mL vial, and the formation of solid precipitate occurred overnight via evaporation. BB, BTS, and BH esylate (BE) were synthesized through a classic slurry crystallization method. Benzocaine and the acids were suspended in a 1:1 molar ratio into 4 mL of acetone at room temperature in a 10 mL closed vial. Moreover, BTS was recrystallized from ACN aiming for an increased crystallinity. Benzocaine−ligustrazine (BL) cocrystal was synthesized through a slow evaporation crystallization method, and the two components were dissolved in a 1:1 molar ratio into 4 mL of acetone at room temperature in a 10 mL closed vial. All the obtained solids were characterized by X-ray powder diffraction (XRPD), differential scanning calorimetry (DSC), thermogravimetric analysis (TGA), and ^{1}H NMR (see Supporting Information, Figures S2−S20). Single-crystal X-ray diffraction (SC-XRD) structures were obtained for BO, BMA, BME, BB, BTS, BL, and BT.

SC-XRD. A summary of data collection and structure refinement for the reported structures is provided in Tables S1−S3. Single-crystal data were collected at 220 K with a Bruker D8 Venture diffractometer equipped with a Photon II detector (Mo Kα: λ = 0.71073 Å; Cu Kα: λ = 1.54184 Å). The intensity data were integrated from several series of exposure frames covering the sphere of reciprocal space. Data reductions were performed with APEX3. Absorption corrections were applied using the program SADABS.[20] The structures were solved by intrinsic phasing with the program SHELXT.[21] Fourier analysis and refinement were performed by the full-matrix least-squares methods based on F^2 using SHELXL-2017[22] implemented in Olex2 software (version 1.3).[23] Nonhydrogen atoms were refined with anisotropic thermal parameters for all crystal structures. The hydrogen atoms of the anions of BMA and BT were located from the difference Fourier map, and they were refined with bond distance restraints. The hydrogen atoms of the amino group of benzocaine of BL and of the protonated amino group of BMA, BT, BME, and BTS were found and refined with bond distance restraints. All of the other hydrogen atoms were placed in their calculated positions. Crystals of BMA were affected by nonmerohedral twinning, and the absorption correction was applied with the TWINABS[24] program. Graphical material was prepared with the Mercury 2021[25] program. Cambridge Structural Database (CSD) search was accomplished on version 5.43 using the ConQuest tool.[26] CCDC 2311937−2311943 contain the supplementary crystallographic data for this paper. These data can be obtained free of charge from The Cambridge Crystallographic Data Centre via www.ccdc.cam.ac.uk/structures.

XRPD. The crystalline state of the samples was investigated by XRPD with an Emyrean Panalytical (UK) V 2.0 instrument equipped with Cu radiation source. Samples were placed on zero background sample holders. The measurements were performed in reflection mode with 2Theta scans from 2.5 to 35°, step size 0.02°, soller slit 0.02 rad, divergence slit 1/8°, and antiscatter slit 1/4°.

Thermal Methods. DSC analyses were performed using a routinely calibrated TA Instruments differential scanning calorimeter Discovery equipped with a computer analyzing system (TRIOS). Indium standard and a sapphire disk were used for temperature/enthalpy calibration and heat capacity calibration, respectively. The system was equipped with a refrigerated cooling system (RCS90) accessory under a dry nitrogen purge (50 mL/min). About 1−5 mg of each sample was placed into a Tzero Aluminum hermetic DSC pan covered with a lid. The sample cell was equilibrated at 0 °C and heated under a nitrogen purge (50 mL/min). All samples were given similar thermal histories by linearly heating to 300 °C at a heating rate of 10 °C/min. 2.6. TGA was performed using a TA Instruments Discovery equipped with a computer analyzing system (TRIOS V4.3). About 2 mg of each sample was placed into a Platinum 100 μL pan. The heating rate was 10 °C/min to 300 °C.

^{1}H NMR. All the NMR experiments were acquired at the ^{1}H proton resonance frequency of 600 MHz, at a temperature of 298 K, using a Bruker AVANCE III HD 600 instrument equipped with a triple resonance TCI INVERSE H-C/N-D-0.5-Z ATMA 5 mm cryoprobe.

Dissolution Studies. Dissolution studies of benzocaine salts and cocrystals were carried out using PBS buffer (pH 7.4) at room temperature. Seven suspensions at a concentration of 1 mg/mL were prepared for every sample. Each suspension corresponds to a different time point (0, 5, 15, 30 min, 1, 2, and 4 h). 200 μL were taken from each sample at the corresponding time point and filtered. Twenty μL from each taken solution were then diluted (1:10) with ACN:H_2O 60:40 and injected into LC/UV/MS system. Each compound was tested in triplicate, in order to monitor the benzocaine concentration in solution at each time point and plot the dissolution rate curve. Ultrahigh-performance liquid chromatography with ultraviolet detection (UHPLC-UV) was used for quantitative analysis of the dissolved drug, which absorbs UV light in the range of 200−290 nm with an absorbance maximum at 273 nm. UHPLC-UV analysis was conducted on a Waters Acquity UPLC system (Milford, MA, USA) that was connected to a diode array detector and equipped with a reversed-phase Kinetex EVO C8 LC column (100 × 2.1 mm; particle size 1.7 μm; pore size 100 Å, Phenomenex). The mobile phase

https://doi.org/10.1021/acs.cgd.3c01488
Cryst. Growth Des. XXXX, XXX, XXX−XXX

consisted of 25 mM of ammonium formate buffer (pH 3) and 0.1% formic acid in ACN, the flow rate was 0.5 mL/min and the column oven was set to 50 °C. The injection volume was 2 μL.

Permeability Studies. Permeability was measured with the Permeapad tool,[27] which is a 96-well plate having a donor and an acceptor compartment with a phosphatidylcholine artificial membrane separating the two compartments. In order to have a complete dissolution, a lag time of 1 h was required (according to the dissolution rate assay) for every sample before filling the donor compartment (200 uL) with the solution (1 mg/mL). The acceptor compartment was filled with 400 uL of pure PBS. The experiment was conducted at room temperature, covering the plate for all of the experiment duration to prevent the degradation of the membrane. At each time point (0, 0.25, 0.5, 1, 2, 4, 6, 8 h), 10 μL of sample was taken and diluted (1:10) with ACN:H_2O 60:40. Each compound was tested in triplicate and injected into LC/UV/MS system. Ultrahigh-performance liquid chromatography with ultraviolet detection (UHPLC-UV) was used for quantitative analysis of the dissolved drug which absorbs UV light in the range of 200−290 nm with an absorbance maximum at 273 nm. UHPLC-UV analysis was conducted on a Waters Acquity UPLC system (Milford, MA, USA) that was connected to a diode array detector and equipped with a reversed phase Kinetex EVO C8 LC column (100 × 2.1 mm; particle size 1.7 μm; pore size 100 Å, Phenomenex). The mobile phase consisted of 25 mM of ammonium formiate buffer (pH 3) and 0.1% formic acid in ACN, the flow rate was 0.5 mL/min, and the column oven was set to 50 °C. The injection volume was 2 μL. Apparent permeability (P_{app}) was calculated as reported by Tzanova et al.[28]

RESULTS AND DISCUSSION

Solid-State Characterization of Salts and Cocrystals. The single crystal structures of BO, BB, BME, BMA, BT, BTS, and BL are reported, and they provide details of the interactions between benzocaine or its protonated form (BH) and its counterpart (anion or coformer). The single-crystal X-ray structural description is divided into three sections: salts containing carboxylic acids, salts with derivatives of sulfonic acids, and the cocrystal (Figure 1).

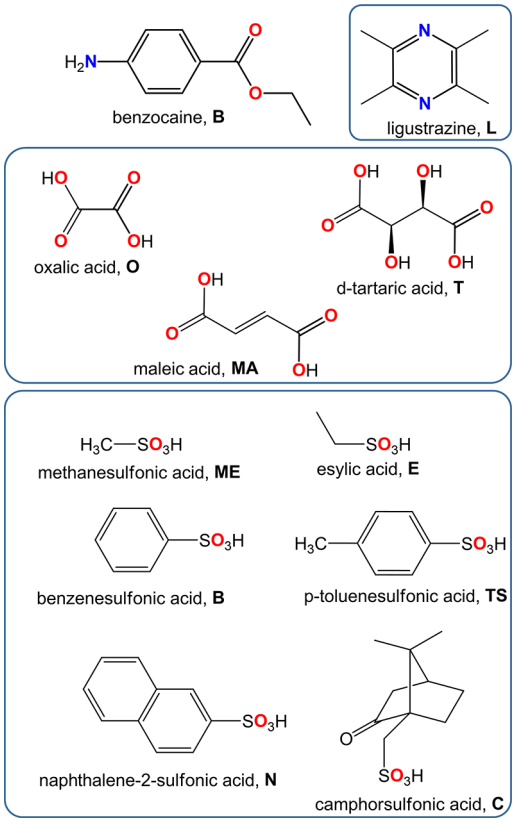

Figure 1. Molecular drawings of benzocaine (API), ligustrazine (coformer), and the various carboxylic and sulfonic acids used as salification agents.

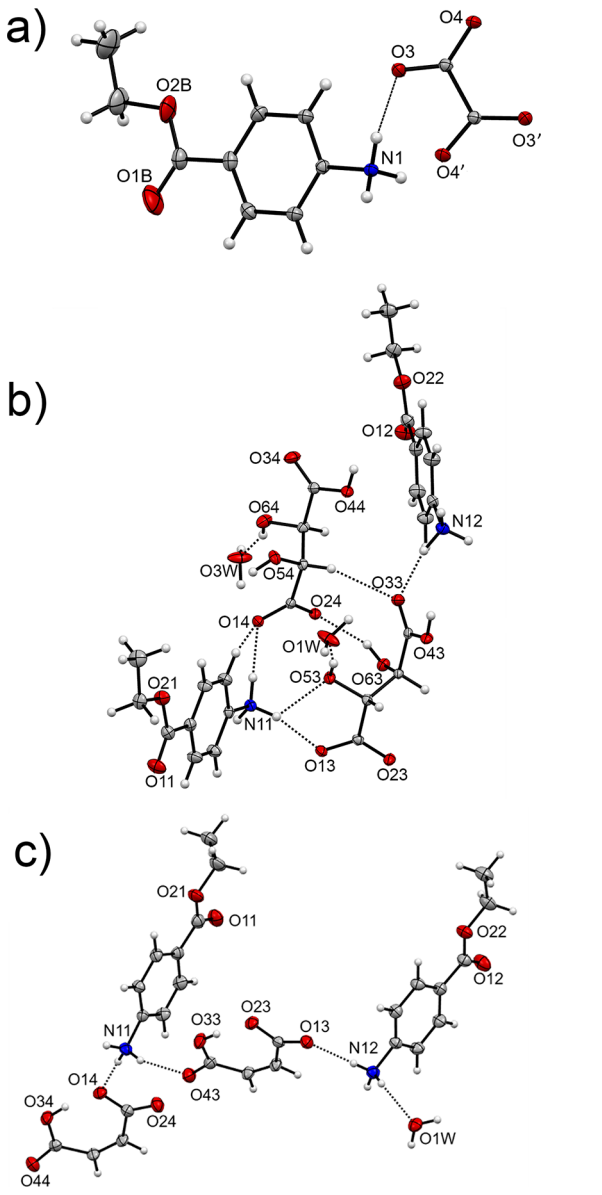

Figure 2. Molecular structures of (a) BO, (b) BT, and (c) BMA. Thermal ellipsoids are depicted at the 30% probability level. Dashed lines represents hydrogen bonds. In BO, oxalate dianion is situated on 2-fold rotation axis, and for BH cation, only one orientation of rotationally disordered COOEt group is shown. Symmetry code: ′ = 1 − x, y, 1/2 − z. In BT, one disordered water molecule of crystallization (close to O3w) is omitted for clarity.

The cocrystal exhibits a benzocaine:ligustrazine 2:1 stoichiometry. Likewise, the salt BO presents a BH:oxalate anions ratio of 2:1, in agreement with the single charge of the cation and of the 2-charge of the oxalate. In all the other systems, the stoichiometry between protonated benzocaine (BH) and the anion is 1:1, according to the presence of monodeprotonated anions. In some compounds, additional water molecules of crystallization are present. In more detail, BMA and BTS

https://doi.org/10.1021/acs.cgd.3c01488
Cryst. Growth Des. XXXX, XXX, XXX−XXX

Table 1. Hydrogen Bonding Geometry in BO, BMA, and BT[a,b]

	D−H···A	d(D−H), Å	d(H−A), Å	d(D−A), Å	D−H−A, °
BO		0.91	1.92	2.789(1)	159.9
	N1−H1B···O4^{2}	0.91	1.89	2.765(1)	161.9
	N1−H1C···O3	0.91	1.88	2.780(1)	169.7
BMA	N11−H11A···O14	0.87(2)	2.03(2)	2.899(4)	177(3)
	N12−H12A···O13	0.87(2)	1.95(2)	2.792(4)	163(4)
	N12−H12B···O23^{3}	0.87(2)	2.03(2)	2.895(4)	172(4)
	N12−H12C···O1W	0.82(2)	2.10(3)	2.821(4)	143(4)
	N11^{10}-H11B···O1W	0.86(2)	2.30(3)	2.936(4)	131(3)
	N11−H11C···O43	0.85(2)	2.04(3)	2.840(4)	155(5)
	O33−H33···O23	0.86(2)	1.59(2)	2.445(3)	170(5)
	O34−H34···O14	0.87(2)	1.56(2)	2.426(3)	172(6)
	O1W−H1WA···O43^{4}	0.87(2)	2.06(3)	2.891(4)	159(5)
	O1W−H1WB···O44^{5}	0.86(2)	2.30(6)	2.896(4)	127(5)
BT	O64−H64···O3W	0.84	1.76	2.553(8)	157.3
	O64−H64···O2W	0.84	1.81	2.649(9)	172.1
	O3W−H3WA···O11^{6}	0.87	2.01	2.856(9)	163.9
	O3W−H3WB···O34^{7}	0.87	1.87	2.738(8)	175.9
	O2W−H2WA···O11^{6}	0.87	2.07	2.885(8)	156
	O2W−H2WB···O34^{7}	0.87	1.95	2.808(9)	168.3
	N11−H11A···O14	0.91(2)	1.84(3)	2.746(4)	173(4)
	N11−H11B···O54^{7}	0.91(2)	1.90(3)	2.788(3)	164(3)
	N11−H11C···O13	0.91(3)	1.83(3)	2.719(4)	166(4)
	O63−H63···O24	0.85(5)	2.01(5)	2.784(3)	151(4)
	N12−H12A···O33	0.94(3)	1.82(3)	2.734(4)	163(5)
	N12−H12B···O64^{8}	0.93(3)	1.92(3)	2.785(4)	154(4)
	N12−H12C···O63^{9}	0.96(3)	1.81(3)	2.765(4)	176(5)
	O43−H43···O23^{9}	0.90(3)	1.58(3)	2.474(3)	174(5)
	O53−H53···O1W	0.85(3)	1.82(3)	2.653(4)	165(4)
	O44−H44···O24^{9}	0.91(3)	1.58(3)	2.482(3)	174(5)
	O1W−H1WB···O13^{9}	0.89(3)	1.91(3)	2.758(3)	158(5)

[a]Symmetry codes: $^{1}1-x, 1+y, 1/2-z$; $^{2}x, -y, 1/2+z$; $^{3}-1+x, +y, +z$; $^{4}-x, -y, 1-z$; $^{5}-1+x, +y, -1+z$; $^{6}2-x, 1/2+y, -z$; $^{7}1+x, +y, +z$; $^{8}+x, +y, 1+z$; $^{9}-1+x, +y, +$; $^{10}1-x, -y, 1-z$. [b]Standard deviations are not present for hydrogen atoms constrained at their idealized positions.

exhibit a 2:2:1 stoichiometry (BH^+:anion$^-$:water), BT exhibit a 1:1:1 stoichiometry (BH^+:anion$^-$:water), whereas BME and BB have a 1:1 BH^+:anion$^-$ stoichiometry as no water of crystallization is present. The ratio between BH and the anions is confirmed by the ^{1}H NMR spectra provided in the Supporting Information. In the case of benzocaine−ligustrazine (BL), the ligustrazine molecule acts as hydrogen bond acceptor with two neutral and independent benzocaine molecules, using both nitrogen sites. On the other hand, BO is unique among the salts containing dicarboxylic acids, as it maintains the acid in a bis-deprotonated state. Oxalic acid is the most acidic among the dicarboxylic acids discussed in this work (oxalic acid: $pK_{a1} = 1.25$, $pK_{a2} = 4.14$; maleic acid $pK_{a1} = 1.94$ $pK_{a2} = 6.22$; tartaric acid: $pK_{a1} = 2.89$, $pK_{a2} = 4.40$.[29] The pronounced acidity of oxalic acid, together with the intricate network of hydrogen bonds surrounding the symmetric structure of the oxalate anion, may promote its occurrence in the doubly deprotonated form.

Benzocaine and Carboxylic Acids. The asymmetric unit of the BO salt comprises one BH molecule and half oxalic acid molecule, which lies on a 2-fold rotation axis. The space group is $P2/c$ with $Z' = 0.5$ and $Z = 2$. Since two distinct entities define the asymmetric unit, the value of Z'' is 2.[30] The overall chemical composition of BO can be described as $(C_9H_{12}NO_2^+)_2\cdot(C_2O_4^{2-})$. The dideprotonated oxalic acid directly interacts via hydrogen bonds with six BH molecules with the shortest distance involving O4 and the nitrogen atom of BH (2.765(1) Å, N1···O4^2, symmetry code $^2 = x, -y, 1/2 + z$). The protonated benzocaine molecules that surround the anion form a $\pi-\pi$ stacking, with the shortest distance between symmetry-related phenyl ring of 3.507(2) Å involving C5 and C6$^{\#}$ (symmetry code $^{\#} = x, 1+y, z$) (Figure S4). The ester group of BH is disordered in two positions having the same occupancy. The disorder is associated with an ideal 180 deg rotation around the single bond connecting the phenyl ring and the ester group.

The asymmetric unit of BMA contains two BH molecules: two maleate anions and one molecule of water (Figure 2). In the description of the molecular structures, we wish to highlight the formulas in order to privilege the stoichiometry of 1 for the BH cations. Since the space group is $P-1$, $Z' = 2$ and $Z = 4$, with five entities comprising the asymmetric unit ($Z'' = 5$). Hence, the chemical composition of BMA is $(C_9H_{12}NO_2^+)\cdot(C_4H_3O_4^-)\cdot 0.5(H_2O)$. The two independent BH molecules exhibit the same conformation of the ester group, and they are connected through two hydrogen bonds to a monodeprotonated maleate anion. The water molecule of crystallization O1w interacts with four distinct molecular entities. Indeed, O1W acts as hydrogen bond acceptor toward two inequivalent BH (N12···O1W, 2.821(4) Å and N11^{10}··· O1W, 2.936(4) Å, ^{10}: $1-x, -y, 1-z$) and as hydrogen bond donor toward two inequivalent anions: O1W···O43^4 (2.891(4) Å, ^{4}: $-x, -y, 1-z$) and O1W···O44^5 (2.896(4) Å, ^{5}: $-1+x, +y, -1+z$) (Figure S5). Both anions exhibit an intramolecular

https://doi.org/10.1021/acs.cgd.3c01488
Cryst. Growth Des. XXXX, XXX, XXX−XXX

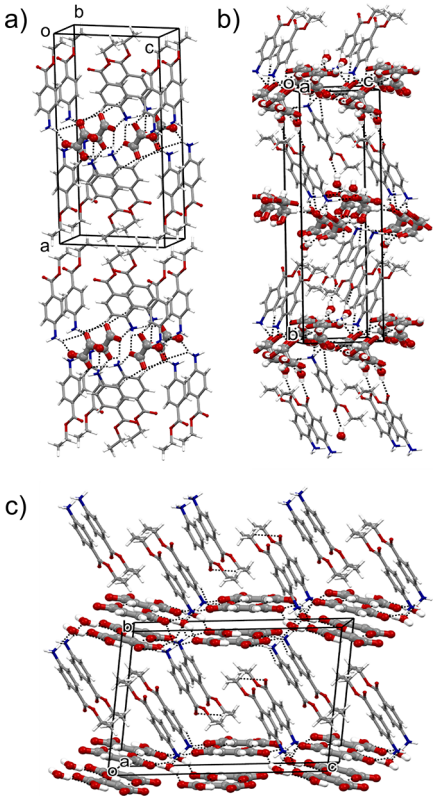

Figure 3. Crystal packing of (a) BO, (b) BT, and (c) BMA, highlighting the interaction between anions and cations (dashed bonds), as viewed along the *b*, *a* and *b*, crystallographic axes, respectively. The anions are depicted with a larger ball and stick size.

hydrogen bond between the protonated and deprotonated carboxylic functions. Table 1 summarizes the hydrogen bonds that occur in the packing.

The structure of BT contains two BH molecules, two monodeprotonated tartrate anions and two water molecules of crystallization, one of which is disordered over two equivalent sites. The space group is $P2_1$ with $Z' = 2$ and $Z = 4$ and with seven molecular entities in the asymmetric unit, $Z'' = 7$. The chemical composition of BT is therefore $(C_9H_{12}NO_2^+)\cdot(C_4H_5O_6^-)\cdot H_2O$. Two tartrate anions are interposed between the two independent BH cations, and the anions are then connected through a hydrogen bond between a hydroxyl function and a carboxylate group (O63···O24, 2.784(3) Å). Both NH_3^+ groups of the two protonated benzocaine molecules act as hydrogen bond donors toward three distinct tartrate anions (Figure S6). One of the two independent water molecules of crystallization accepts a hydrogen bond from the hydroxyl groups of a tartrate anions (O53···O1W 2.653(4) Å). The second water molecule is disordered in two sites (O2W and O3W), and the two fragments accept a hydrogen bond from the hydroxyl group of the second tartrate anion (O64···O3W, 2.553(8) Å and O64···O2W, 2.649(9) Å).

The inspection of the crystal packing shows that BO, BT, and BMA exhibit a layered arrangement of cations and anions, having distinct zones occupied by carboxylate moieties and BH entities (Figure 3). In the three structures, BH cations exhibit a partial stacking with the aromatic moieties. In more detail, in BO, the cations are organized in a columnar head-to-head fashion, whereas in BMA and BT they adopt a head-to-tail arrangement, see Figures S4–S6.

Benzocaine and Sulfonic Acids. BME crystallizes in the $P2_1/c$ space group, and the asymmetric unit contains two BH molecules and two mesylate anions (Figure 4). Hence, $Z' = 2$, $Z = 8$ with the chemical composition of $(C_9H_{12}NO_2^+)\cdot(CH_3O_3S^-)$. One of the two BH cations presents a disorder on the ester group, which is related to two different but similar conformation of the peripheral ethyl residue. Compound BB crystallizes in P−1 and the asymmetric unit contains two BH cations and two benzenesulfonate anions, with $Z' = 2$, $Z = 4$, with the chemical composition of $(C_9H_{12}NO_2^+)\cdot(C_6H_5O_3S^-)$. In both, BME and BB, four distinct molecules comprise the asymmetric so that $Z'' = 4$. BME and BB show a similar structural organization and supramolecular connectivity: the two independent BH molecules interact with four anion molecules and each anion interacts with four BH cations acting as a bridge between protonated benzocaine molecules in the packing (Figures S7 and S8). More specifically, in BME, O24 and O14 are connected to N12 and N11, respectively, via HBs, whereas O34 is engaged in two HBs with symmetry-related N11 and N12. Likewise, the second anion forms HBs with N11 and N12 with O33 and O23, respectively, and the third oxygen atom O13 forms two HBs with N12 and N11. The interactions N11···O33/N11···O34 and N12···O24/N12···O13 can be described as bifurcated hydrogen bonds (see Figure S7). The donor−acceptor HBs distance is in the 2.748(3)−2.921(3) Å range (Table 2). In BB, N11 forms HBs with four oxygen atoms O14, O34 O23, and O13, whereas N12 interacts through HBs with O14, O33 O24 and a symmetry-related O33. The interaction N11···O23 and N12···O24 can be described as bifurcated hydrogen bonds (see Figure S8). The donor−acceptor HBs distance is in the 2.740(2)−3.015(2) Å range (Table 2).

The asymmetric unit of BTS contains two BH molecules: two *p*-toluenesulfonate anions and one water molecule of crystallization. One of the two BH presents a disorder on the ester group similarly to BME. The space group is $P2_1/n$ with $Z' = 2$ and $Z = 4$ and with five molecular entities in the asymmetric unit ($Z'' = 5$). The chemical composition of BTS is $(C_9H_{12}NO_2^+)\cdot(C_7H_7O_3S^-)\cdot 0.5(H_2O)$ (Figure 4). The BTS network is slightly more complex than that of BME and BB since it involves an additional water molecule. In more detail, N11 of the first BH interacts with four oxygen atoms of four *p*-toluenesulfonate anions by forming HBs with O14, O24, O33, and O44. The interaction with O34 and O33 is a bifurcated HB. N12 forms three HBs with O13 and two symmetry-related O24 oxygen atoms. N12 also acts as HB donor toward the water molecule through a bifurcated HB. The donor−acceptor HBs distance is in the 2.753(3)−2.986(3) Å range (Table 2).

The packing of BME exhibits a layered arrangement similar to that of BO, with interactions occurring between the terminal ethyl ester groups of symmetry-related protonated benzocaine molecules. Differently from BO, the BH cation of BME does not form $\pi-\pi$ stacking, but the molecules are arranged in an edge-to-face fashion. BB also shows a layered structure, quite similar to that of BT and BMA involving the carboxylate anions previously described. In BB, the BH cations are arranged in a head-to-tail fashion, whereas the aromatic ring of the benzenesulfonate anions leads to CH···π interactions between nearby molecules (Figure 5). The packing of BTS, as viewed along the b crystallographic axis, shows one BH cation surrounded by aromatic groups of the anions. The second independent BH cation forms a head-to-tail arrangement

https://doi.org/10.1021/acs.cgd.3c01488
Cryst. Growth Des. XXXX, XXX, XXX−XXX

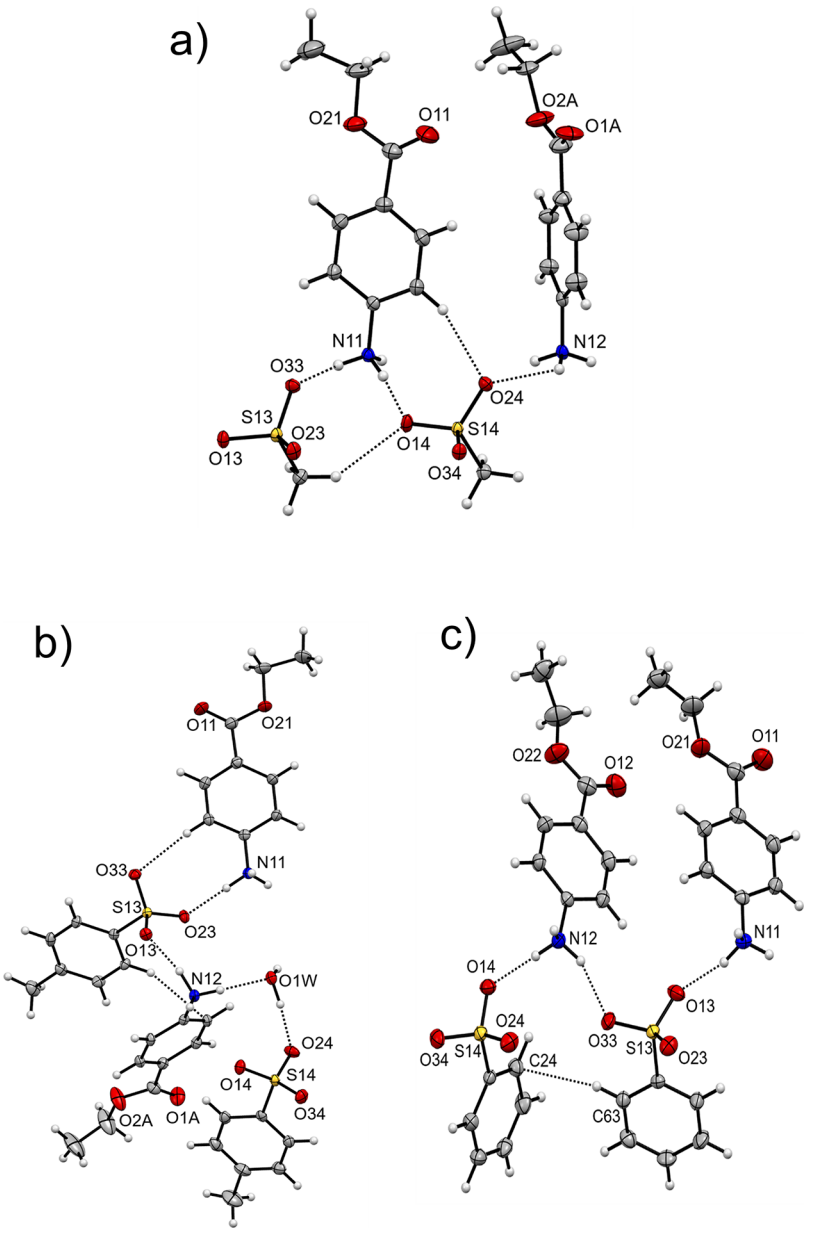

Figure 4. Asymmetric units of (a) BME, (b) BTS, and (c) BB. Thermal ellipsoids are depicted at the 30% probability level. Dashed lines represent hydrogen bonds. The asymmetric units of the three systems comprise two cations and two anions, and in BTS a water molecule of crystallization is also present. In BT and BTS, one of the two cations exhibits a rotational disorder of the ester group (only one fragment is shown for clarity).

without $\pi-\pi$ stacking in similar disposition to that of BME (see Figures 5 and S9).

Benzocaine–Ligustrazine Cocrystal. The asymmetric unit of the BL cocrystal contains two symmetry-independent benzocaine molecules and one ligustrazine molecule. The space group is $C2/c$ with $Z' = 1$, $Z = 8$, and $Z'' = 3$, and the chemical composition is $(C_9H_{11}NO_2)_2 \cdot C_8H_{12}N_2$ (Figure 6). Both independent benzocaine molecules act as HB donors toward the ligustrazine molecule and toward the C=O group of a symmetry-related benzocaine (Figure S10). The four HBs involving the two amino groups N11 and N12 present a donor–acceptor range of 2.888(2)–3.142(2) Å, which is significantly greater than the average HBs distance found in the ionic systems previously described (with carboxylate or sulfonate anions) (Table 3). Hence, in BL, despite an almost linear D–H···A angle (164(2)–174(2) deg. range), it may be assumed that the HBs are weaker than in the ionic systems. The crystal packing shows one benzocaine molecules forming an alternate π-stacking with ligustrazine (depicted in orange in Figure 6) with the minimum distance found between C52··· N23$^{¥}$ (3.460(2) Å, $^{¥}$: $-x + 1/2 + 1, +y + 1/2, -z + 1/2$). The second benzocaine molecule is arranged in a head-to-tail fashion giving rise to a π-stacking with the closest contact between C31 and C71§ (3.512(3) Å, §: $-x + 2, -y + 1, -z + 1$).

The value of Z″ in the structures reported in the work varies from 2 (minimum value for a salt or cocrystal) to 7. Values of Z″ greater than 2 for these systems could be associated with the need to maximize the interactions between the various components in the solid state. Indeed, the presence of a greater number of chemically equal but independent components would facilitate a more efficient crystalline packing in analogy to the assumptions that lead to having $Z' > 1$.[31]

https://doi.org/10.1021/acs.cgd.3c01488
Cryst. Growth Des. XXXX, XXX, XXX–XXX

Table 2. Hydrogen Bonding Geometry in BME, BT, and BTS[a,b]

	D−H···A	d(D−H), Å	d(H−A), Å	d(D−A), Å	D−H−A, °
BME	N12−H12A···O24	0.82(3)	2.34(3)	2.886(3)	125(2)
	N12−H12B···O23	0.96(3)	1.81(3)	2.773(3)	175(3)
	N12−H12C···O34[1]	0.92(3)	1.92(3)	2.834(3)	172(3)
	N12−H12A···O13[7]	0.82(3)	2.21(3)	2.921(3)	145(3)
	N11−H11A···O13	0.93(3)	1.89(3)	2.821(3)	175(3)
	N11−H11B···O14	0.92(3)	1.83(3)	2.748(3)	173(3)
	N11−H11C···O33[2]	0.87(3)	2.30(3)	2.876(3)	124(3)
	N11−H11C···O34[8]	0.87(2)	2.13(3)	2.900(3)	148(3)
BB	N12−H12A···O14	0.91	1.89	2.799(2)	178.9
	N12−H12B···O33[3]	0.91	1.97	2.804(2)	151.9
	N12−H12C···O33	0.91	1.91	2.764(2)	156.5
	N12−H12B···O24[9]	0.91	2.61	3.015(2)	107.4
	N12−H12C···O24[9]	0.91	2.76	3.015(2)	97.2
	N11−H11A···O13	0.91	1.85	2.740(2)	166.6
	N11−H11B···O34[3]	0.91	2.01	2.847(2)	151.6
	N11−H11C···O14[8]	0.91	2.02	2.908(2)	173.5
	N11−H11B···O23[10]	0.91	2.41	2.868(2)	111.0
	N11−H11C···O23[10]	0.91	2.60	2.868(2)	98.1
BTS	N11−H11A···O14[4]	0.91(3)	1.95(3)	2.858(3)	174(3)
	N11−H11B···O33[5]	0.89(3)	2.13(3)	2.822(3)	134(2)
	N11−H11C···O23	0.95(3)	1.83(3)	2.782(3)	178(3)
	N11−H11B···O34[11]	0.89(3)	2.31(3)	2.986(3)	132(3)
	N12−H12A···O1W	0.93(3)	1.85(3)	2.779(3)	178(3)
	N12−H12B···O13	1.02(3)	1.79(3)	2.794(3)	169(3)
	N12−H12C···O24[6]	0.90(3)	2.08(3)	2.881(3)	147(3)
	N12−H12A···O1W[4]	0.93(3)	2.69(3)	2.907(3)	94(3)
	N12−H12C···O1W[4]	0.90(3)	2.57(3)	2.907(3)	103(3)
	O1W−H1WA···O13[5]	0.81(3)	2.08(3)	2.827(2)	154(3)
	O1W−H1WB···O24	1.00(4)	1.76(4)	2.753(3)	173(3)

[a]Symmetry codes: [1]+x, −1 + y, +z; [2]+x, 1 + y, +z; [3]1 − x, 1 − y, 2 − z; [4]1 − x, 1 − y, 1 − z; [5]+x, −1 + y, +z; [6]+x, 1 + y, +z; [7] 1 + x, +y, +z; [8]−1 + x, +y, +z; [9]1 − x, 1 − y, 2 − z; [10]−x, 1 − y, 2 − z; [11]1 − x, −y, 1 − z. [b]Standard deviations are not present for hydrogen atoms constrained at their idealized positions.

In order to thoroughly characterize the bulk material obtained by salification or cocrystallization, the XRPD patterns (Figure S11) of benzocaine are compared to that of the adducts, revealing complete conversion of the starting materials. Consistently, the thermal behavior, studied through DSC and TGA (Figures S13−S15), showed distinct features associated with the adducts formation, such as a different melting temperature compared to benzocaine alone (Table 4).

Dissolution Studies. The dissolution rate of a substance is a critical factor in pharmaceutical formulations, especially for topical administration. The measurements involved monitoring the concentration of benzocaine for every adduct (benzocaine, benzocaine salts, and cocrystal) over time in a biomimetic solution at pH 7.4 PBS. This assessment evaluated the rate of benzocaine accumulation in the solution, and specifically on its concentration during the unsaturation regime. Conversely, solubility would refer to the amount of benzocaine at the equilibrium, after a prolonged time in the saturation regime. The dissolution experiment lasted 4 h (Figure 7), and quite interestingly, each new system demonstrated an enhanced dissolution rate compared to benzocaine alone. The accelerated dissolution rate of the adducts (salts and cocrystals) increased the availability of benzocaine in the medium, facilitating potential absorption, which is particularly crucial during the early hours of topical administration. In fact, at 15 min, every system had reached a higher percentage of dissolved drug compared to benzocaine alone. Indeed, BME, BE, BTS, BC, BN, and BB had already reached the 1 mg/mL value, whereas BO, BL, BT, and BMA showed a slightly slower dissolution rate (approximately 0.8 mg/mL). In other words, the carboxylates seemed to dissolve slower than the sulfonates. This observation seems to be in contrast with the higher values of the melting points of the sulfonates, which is usually associated with a greater stability of the solid-state interaction and a higher crystal lattice energy.[32] Indeed, despite the higher melting points, the sulfonate salts had the fastest dissolution rate.

Benzocaine alone showed the slowest dissolution profile, since it exhibited a concentration of 0.54 mg/mL after 1 h, while all the other systems were completely dissolved reaching the plateau of 1 mg/mL in approximately 0.5 h.

Permeability Studies. Permeability studies are useful to elucidate the impact of salification and cocrystallization on the diffusion of benzocaine through a membrane. Indeed, substances with a high permeability coefficient are characterized by an efficient absorption since they are rapidly translocated across biological membranes. The possible modulation of the permeability coefficient of benzocaine is crucially important in the attempt to increase the duration of action of benzocaine. The experiment monitored the accumulation of benzocaine in the acceptor compartment over time. Following the measurement of its concentration and the calculation of the rate of diffusion, the apparent permeability (P_{app})[33] could be calculated as the steady-state

https://doi.org/10.1021/acs.cgd.3c01488
Cryst. Growth Des. XXXX, XXX, XXX−XXX

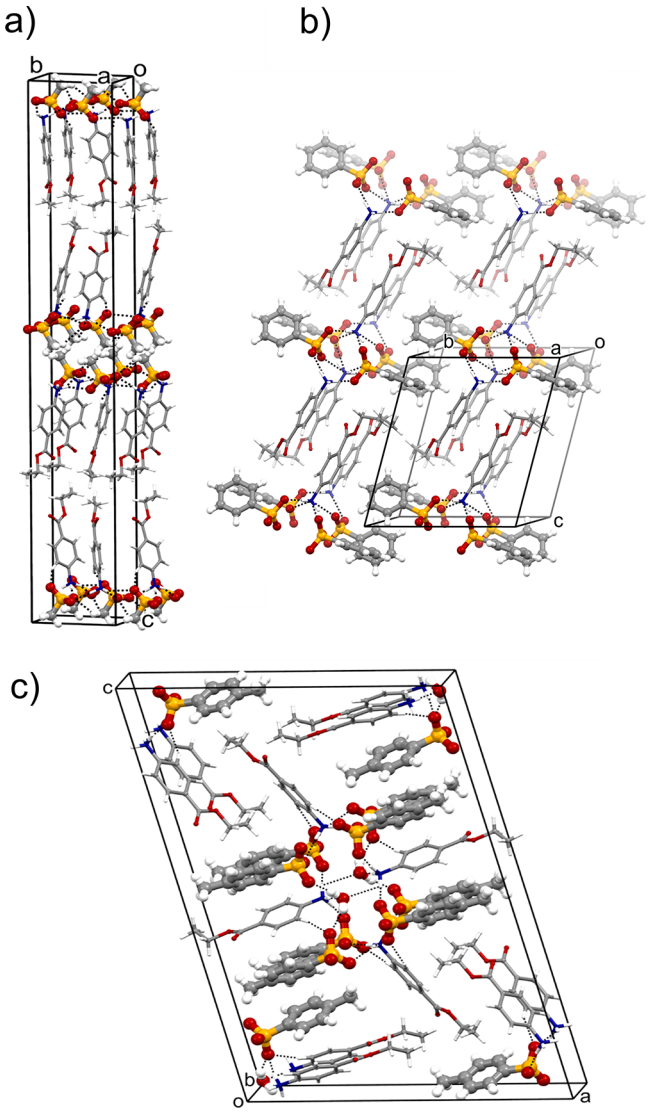

Figure 5. Crystal packing of (a) BME, (b) BB, and (c) BTS, highlighting the interaction between anions and cations (dashed bonds), as viewed along the *a*, *a*, and *b* crystallographic axes, respectively. The anions are depicted with a larger ball and stick size.

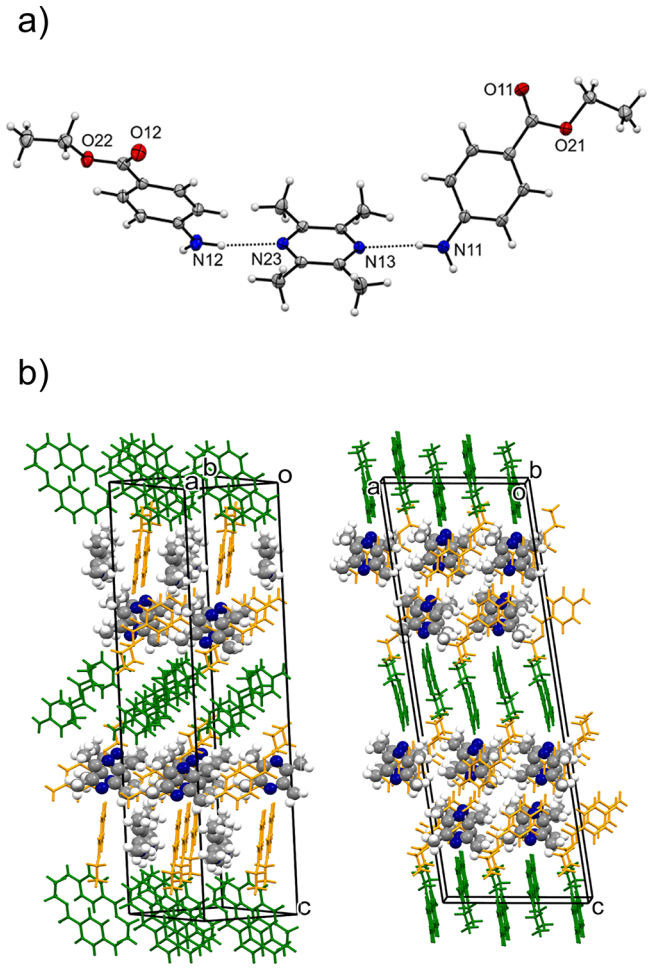

Figure 6. (a) Molecular structure of BL with thermal ellipsoids depicted at the 30% probability level. The asymmetric unit comprises two benzocaine and one ligustrazine molecule. Dashed lines represents hydrogen bonds. (b) Crystal packing of BL, highlighting the interaction between benzocaine and the coformer. The two independent benzocaine molecules of the asymmetric unit are highlighted in green and yellow, respectively.

flux divided by the initial concentration in the donor chamber. For the experiment, the samples used were fully dissolved before being introduced into the donor compartment, ensuring that the sample preparation step rendered permeability independent of the dissolution rate.

Frequently, excipient molecules called chemical permeation enhancers like transcutol are employed to increase the P_{app} as they interact with the constituents of the skin.[8,34] In our approach, we investigated the effect of salification on the P_{app}. Interestingly, as shown in Figure 8, all the systems showed a different and increased P_{app} in the tested medium (Table S5 reports the results for every repetition). Hence, the complex formed between benzocaine and its counterpart in solution promoted the modulation of benzocaine's permeability. Sulfonic acids seemed to be the most effective in increasing the diffusion through the lipid membrane; in particular, BN, BB, BTS, and BC had the highest P_{app}. Nevertheless, BME and BE were not equally successful, and presumably the lower lipophilicity of methanesulfonic acid and ethanesulfonic acid seemed to be crucial. Indeed, by plotting the P_{app} as a function of the Log *P* of the neutral counterpart, it seems that for intermediate Log *P* values and in the 0.59−1.05 range, the P_{app} has the highest values (corresponding to BB, BTS, and BC) (Figure 9). On the one hand, when the system is too hydrophilic, P_{app} shows smaller values in the series; on the other hand, when the system is too hydrophobic, the P_{app} starts decreasing. However, it is worth noticing that more points in the series would be required to identify the proper correlation between P_{app} and Log *P*. In summary, the lipophilic nature of benzocaine (Table 5) and its derivatives played a crucial role in dictating the membrane diffusion rates, as it affected the solubility and the partitioning of the drug within the lipid membrane.[35,36]

Interestingly, despite ligustrazine exhibits an intermediate (and presumably favorable) lipophilicity, the cocrystal BL showed only a modest P_{app}. The low permeability of BL may be explained by the different strength of the interactions formed by benzocaine and ligustrazine on the one side and by the BH cations and the anions on the other side. Indeed, it is reasonable to assume that the hydrogen bond in BL is weaker than the hydrogen bond found in the ionic pairs, since in the latter cases, it is supported by the net charge of the two

https://doi.org/10.1021/acs.cgd.3c01488
Cryst. Growth Des. XXXX, XXX, XXX−XXX

Table 3. Hydrogen Bonding Geometry in the BL Cocrystal[a]

D−H···A	d(D−H), Å	d(H−A), Å	d(D−A), Å	D−H−A, °
N12−H12A···N23	0.91(2)	2.22(2)	3.133(2)	171(2)
N11−H11A···N13	0.89(2)	2.18(2)	3.056(2)	170(2)
N11−H11B···O11[1]	0.87(2)	2.02(2)	2.888(2)	172(2)
N12−H12B···O12[2]	0.89(2)	2.28(2)	3.142(2)	164(2)

[a]Symmetry codes: [1]$+x, -1+y, +z$; [2]$1/2+x, -1/2+y, +z$.

Table 4. Melting Temperature of Benzocaine, Ligustrazine, Acids, Benzocaine−Ligustrazine Cocrystal, and Benzocaine Salts

compound	melting temp. (°C)
benzocaine	**89**
BH maleate (BMA)	96
maleic acid	130
BH mesylate (BME)	211
methanesulfonic acid	20
BH oxalate (BO)	135
oxalic acid	365
BH esylate (BE)	157
ethanesulfonic acid	−17
BH tartrate (BT)	149
L-(+)-tartaric acid	170
BH naphthalenesulfonate (BN)	217
naphthalenesulfonic acid	140
BH benzenesulfonate (BB)	200
benzenesulfonic acid	65
BH *p*-toluenesulfonate (BTS)	185
p-toluenesulfonic acid	104.5
BH camphorsulfonate (BC)	n.d.[a]
(1*S*)-(+)-camphorsulfonic acid	196
benzocaine ligustrazine (BL)	84
ligustrazine	84

[a]Complex thermal behavior.

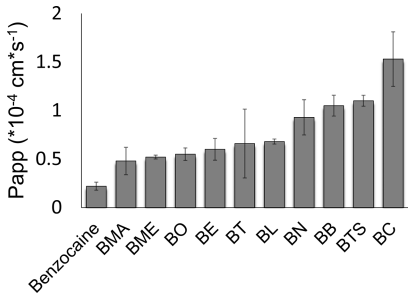

Figure 8. Apparent permeability of benzocaine, BC, BO, BB, BE, BL, BN, BTS, BT, BME, and BMA.

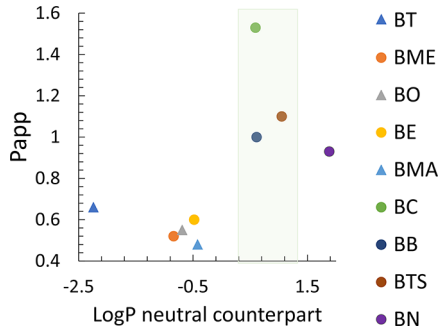

Figure 9. P_{app} and Log P of the neutral counterpart are plotted in the graph (○ for salts of benzocaine with sulfonic acids and △ for salts of benzocaine with carboxylic acids), highlighting the range where the Log P is most favorable (0.59−1.05) in increasing the permeability of the final adduct.

521 interacting charged entities. This is also supported by the
522 intermolecular distance found in the crystal structures between
523 the donor and acceptor in the HBs, which is the longest for BL.
524 As a result, it can be proposed that a weaker intermolecular
525 interaction in BL would limit the survival of the adduct in
solution, and consequently the ability of ligustrazine to 526
modulate the P_{app} of benzocaine. 527

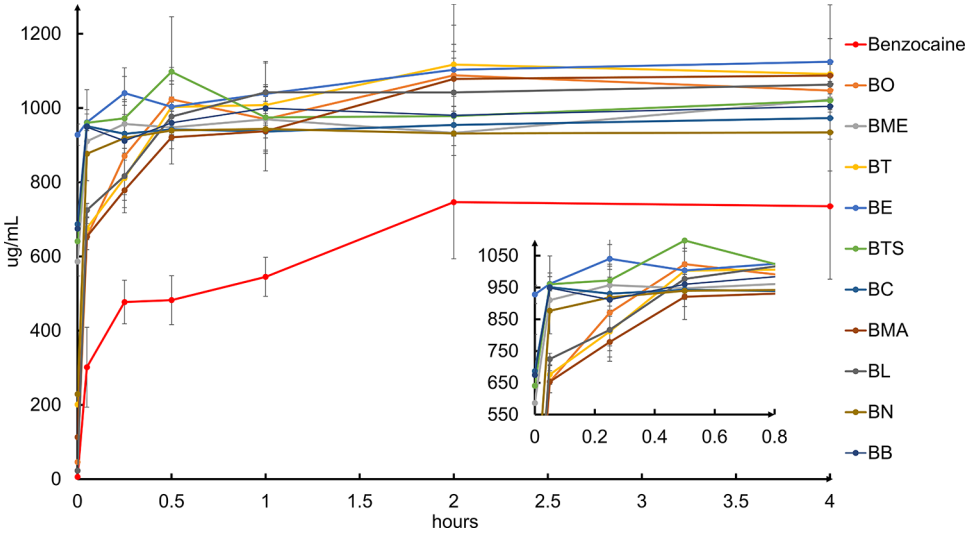

Figure 7. Dissolution profiles of BC, BO, BB, BE, BL, BN, BTS, BT, BME, and BMA in PBS up to 4 h.

https://doi.org/10.1021/acs.cgd.3c01488
Cryst. Growth Des. XXXX, XXX, XXX−XXX

Table 5. Apparent Permeability P_{app} ($\times 10^{-4}$ cm s^{-1}) of BC, BO, BB, BE, BL, BN, BTS, BT, BME, and BMA; Log *P* of the Acids (Maleic, Oxalic, L-(+)-Tartaric, Methanesulfonic, Ethanesulfonic, 2-Naphthalenesulfonic, Benzenesulfonic, *p*-Toluenesulfonic, Camphorsulfonic), and the Coformer Ligustrazine

compound	Log P^a	P_{app} ($\times 10^{-4}$ cm s^{-1})
benzocaine		0.22
BH tartrate (BT)	−2.24	0.66
BH mesylate (BME)	−0.84	0.52
BH oxalate (BO)	−0.69	0.55
BH esylate (BE)	−0.48	0.60
BH maleate (BMA)	−0.42	0.48
BH camphorsulfonate (BC)	0.59	1.53
BH benzenesulfonate (BB)	0.61	1.05
BH *p*-toluenesulfonate (BTS)	1.05	1.10
BH naphthalenesulfonate (BN)	1.88	0.93
benzocaine ligustrazine (BL)	*0.78*	*0.68*

[a]The values are relative to the undissociated acids and ligustrazine.

CONCLUSIONS

In this work, we have investigated the formation of salts and a cocrystal to address the pharmacokinetic challenges associated with benzocaine. Benzocaine is known for its low duration of action due to rapid metabolism and elimination from the body, resulting in a short-lived anesthetic effect. Crystal engineering was employed as a strategy to mitigate this issue.

We report the characterization of nine new salts and one cocrystal of benzocaine, and we illustrate their solid-state features analyzed by means of single-crystal and powder X-ray diffraction and thermal methods. In the presence of acid moieties, benzocaine is protonated on the aromatic amino group, giving rise to the formation of ionic pairs sustained by hydrogen bonds between the oxygen atoms of the organic acids (carboxylic or sulfonic) and the protonated amino group. The only cocrystal analyzed is with ligustrazine as coformer, and in this case, there is the formation of hydrogen bonds between the amino group of benzocaine and both the nitrogen atoms of ligustrazine. Dissolution and permeability studies revealed improved dissolution rate and permeability for the newly synthesized compounds, suggesting their potential for improved delivery of benzocaine. Indeed, in the first critical 15−30 min, every newly synthesized system was dissolved completely (1 mg/mL), with the fastest being the sulfonates salts, while benzocaine alone dissolved with a maximum concentration of 0.54 mg/mL and with a good part still suspended. Another important aspect to consider when evaluating the pharmacokinetic profile of a substance is the determination of its permeability, which is the ability to cross a bilayer membrane. An optimal permeability profile is associated with the accumulation of the substance in a compartment where it can express its function. All of the tested adducts showed an increase of permeability in the 1.5−7-fold range with respect to benzocaine alone. Interestingly, three sulfonic acid derivatives were the most effective, namely BB (5-fold increase), BTS (5-fold increase), and BC (7-fold increase). Therefore, in terms of developability, lipophilic sulfonic acids appear to be the most suitable counterions, considering the melting point, dissolution rate, and permeability of the final drug candidate. These findings underscore the effectiveness of crystal engineering in tailoring the dissolution rate and permeability of active pharmaceutical ingredients, which can ultimately impact their in vivo performance. Further exploration of crystal engineering approaches holds promise for optimizing the therapeutic outcomes and patient experiences associated with benzocaine and similar compounds.

ASSOCIATED CONTENT

Supporting Information

The Supporting Information is available free of charge at https://pubs.acs.org/doi/10.1021/acs.cgd.3c01488.

Crystallographic tables, 2D fingerprint plots, single crystal structure, XRPD patterns, DSC and TGA thermograms, NMR spectra, and apparent permeability (PDF)

Accession Codes

CCDC 2311937−2311943 contain the supplementary crystallographic data for this paper. These data can be obtained free of charge via www.ccdc.cam.ac.uk/data_request/cif, or by emailing data_request@ccdc.cam.ac.uk, or by contacting The Cambridge Crystallographic Data Centre, 12 Union Road, Cambridge CB2 1EZ, UK; fax: +44 1223 336033.

AUTHOR INFORMATION

Corresponding Author

Luciano Marchiò − *Department of Chemistry, Life Sciences and Environmental Sustainability, University of Parma, 43124 Parma, Italy; Biopharmanet TEC, Università di Parma, 43124 Parma, Italy;* orcid.org/0000-0002-0025-1104; Email: luciano.marchio@unipr.it

Authors

Laura Baraldi − *Department of Chemistry, Life Sciences and Environmental Sustainability, University of Parma, 43124 Parma, Italy; Preclinical Analytics and Early Formulations Department, Chiesi Farmaceutici S.p.A., 43123 Parma, Italy;* orcid.org/0000-0003-1353-8996

Irene Bassanetti − *Preclinical Analytics and Early Formulations Department, Chiesi Farmaceutici S.p.A., 43123 Parma, Italy*

Francesco Amadei − *Preclinical Analytics and Early Formulations Department, Chiesi Farmaceutici S.p.A., 43123 Parma, Italy*

Alessia Bacchi − *Department of Chemistry, Life Sciences and Environmental Sustainability, University of Parma, 43124 Parma, Italy; Biopharmanet TEC, Università di Parma, 43124 Parma, Italy;* orcid.org/0000-0001-5675-9372

Complete contact information is available at: https://pubs.acs.org/10.1021/acs.cgd.3c01488

Notes

The authors declare no competing financial interest.

ACKNOWLEDGMENTS

Chiesi Farmaceutici SpA is acknowledged for funding this work and for the support of the D8 Venture X-ray equipment. This work also benefited from the equipment and framework of the COMP-HUB and COMP-R Initiatives, funded by the "Departments of Excellence" program of the Italian Ministry for University and Research (MIUR, 2018-2022 and MUR, 2023-2027).

REFERENCES

(1) Khair-ul-Bariyah, S.; Arshad, M.; Ali, M.; Din, M. I.; Sharif, A.; Ahmed, E. Benzocaine: Review on a Drug with Unfold Potential. *Mini-Reviews Med. Chem.* **2020**, *20* (1), 3−11.

(2) Lee, H.-S. Recent Advances in Topical Anesthesia. *J. Dent. Anesth. Pain Med.* **2016**, *16* (4), 237.

(3) De Melo, N. F.; De Araújo, D. R.; Grillo, R.; Moraes, C. M.; De Matos, A. P.; de Paula, E.; Rosa, A. H.; Fraceto, L. F. Benzocaine-Loaded Polymeric Nanocapsules: Study of the Anesthetic Activities. *J. Pharm. Sci.* **2012**, *101* (3), 1157−1165.

(4) Üstündağ Okur, N.; Çağlar, E. Ş.; Arpa, M. D.; Karasulu, H. Y. Preparation and Evaluation of Novel Microemulsion-Based Hydrogels for Dermal Delivery of Benzocaine. *Pharm. Dev. Technol.* **2017**, *22* (4), 500−510.

(5) Mura, P.; Maestrelli, F.; González-Rodríguez, M. L.; Michelacci, I.; Ghelardini, C.; Rabasco, A. M. Development, Characterization and in Vivo Evaluation of Benzocaine-Loaded Liposomes. *Eur. J. Pharm. Biopharm.* **2007**, *67* (1), 86−95.

(6) Puglia, C.; Sarpietro, M. G.; Bonina, F.; Castelli, F.; Zammataro, M.; Chiechio, S. Development, Characterization, and in Vitro and in Vivo Evaluation of Benzocaine- and Lidocaine-Loaded Nanostructrured Lipid Carriers. *J. Pharm. Sci.* **2011**, *100* (5), 1892−1899.

(7) Shin, S. C.; Lee, J. W.; Yang, K. H.; Lee, C. H. Preparation and Evaluation of Bioadhesive Benzocaine Gels for Enhanced Local Anesthetic Effects. *Int. J. Pharm.* **2003**, *260* (1), 77−81.

(8) De Araujo, D. R.; Padula, C.; Cereda, C. M. S.; Tófoli, G. R.; Brito, R. B.; De Paula, E.; Nicoli, S.; Santi, P. Bioadhesive Films Containing Benzocaine: Correlation between in Vitro Permeation and in Vivo Local Anesthetic Effect. *Pharm. Res.* **2010**, *27* (8), 1677−1686.

(9) Ferreira, L.; Campos, J.; Veiga, F.; Cardoso, C.; Paiva-Santos, A. C. Cyclodextrin-Based Delivery Systems in Parenteral Formulations: A Critical Update Review. *Eur. J. Pharm. Biopharm.* **2022**, *178*, 35−52.

(10) Gana, I.; Barrio, M.; Do, B.; Tamarit, J. L.; Céolin, R.; Rietveld, I. B. Benzocaine Polymorphism: Pressure-Temperature Phase Diagram Involving Forms II and III. *Int. J. Pharm.* **2013**, *456* (2), 480−488.

(11) Rodriguez-Caabeiro, F.; Criado-Fomelio, A.; Jimenez-Gonzalez, A.; Guzman, L.; Igual, A.; Perez, A.; Pujol, M. Experimental Chemotherapy and Toxicity in Mice of Three Mebendazole Polymorphic Forms. *Chemotherapy* **1987**, *33* (4), 266−271.

(12) Rodríguez-Spong, B.; Price, C. P.; Jayasankar, A.; Matzger, A. J.; Rodríguez-Hornedo, N. General Principles of Pharmaceutical Solid Polymorphism: A Supramolecular Perspective. *Adv. Drug Delivery Rev.* **2004**, *56* (3), 241−274.

(13) Desiraju, G. R. *Crystal Engineering: The Design of Organic Solids*; Elsevier Sci.: 1989; pp 312.

(14) Nangia, A. K.; Desiraju, G. R. Crystal Engineering: An Outlook for the Future. *Angew. Chemie - Int. Ed.* **2019**, *58* (13), 4100−4107.

(15) Ji, X.; Wu, D.; Li, C.; Li, J.; Sun, Q.; Chang, D.; Yin, Q.; Zhou, L.; Xie, C.; Gong, J.; Chen, W. Enhanced Solubility, Dissolution, and Permeability of Abacavir by Salt and Cocrystal Formation. *Cryst. Growth Des.* **2022**, *22* (1), 428−440.

(16) Wu, B.-C.; Dai, X.-Y.; Xiao, F.-P.; Jin, L.-F. 4-(Ethoxycarbonyl)-Anilinium Chloride. *Acta Crystallogr., Sect. E: Crystallogr. Commun.* **2006**, *E62* (2), 4327−4328.

(17) Manjunatha, N. K.; Alzubaidy, N. N.; Likhitha, U.; Manjunatha, M.; Saravanan, K.; Krishna Reddy, B. V.; Kannika, B. R.; Somashekarachar, G.; Swamy, M. T.; Siddaraju, B. P.; Nagendra, P.; Rajesha; Madan Kumar, S. A Potent Anesthetic Drug Salt: Experimental and Computational Studies. *J. Mol. Struct.* **2022**, *1263*, No. 133049, DOI: 10.1016/j.molstruc.2022.133049.

(18) Henck, J. O.; Bernstein, J.; Ellern, A.; Boese, R. Disappearing and Reappearing Polymorphs. The Benzocaine:Picric Acid System. *J. Am. Chem. Soc.* **2001**, *123* (9), 1834−1841.

(19) Pletcher, J.; Sax, M.; Yoo, C. S. The Crystal Structure of 4-Ethoxycarbonylanilinium Bis- p -Nitrophenylphosphate. *Acta Crystallogr. Sect. B* **1972**, *28* (2), 378−387.

(20) Sheldrick, G. M. *SADABS-2008/1 - Bruker AXS Area Detect. Scaling Absorpt. Correct*; Bruker AXS Madison: Wisconsin, USA, 2008.

(21) Sheldrick, G. M. SHELXT - Integrated Space-Group and Crystal-Structure Determination. *Acta Crystallogr. Sect. A Found. Crystallogr.* **2015**, *71* (1), 3−8.

(22) Sheldrick, G. M. Crystal Structure Refinement with SHELXL. *Acta Crystallogr. Sect. C Struct. Chem.* **2015**, *71*, 3−8.

(23) Dolomanov, O. V.; Bourhis, L. J.; Gildea, R. J.; Howard, J. A. K.; Puschmann, H. OLEX2: A Complete Structure Solution, Refinement and Analysis Program. *J. Appl. Crystallogr.* **2009**, *42* (2), 339−341.

(24) Sheldrick, G. M. *TWINABS 2012/*; Bruker: Madison, Wisconsin, USA, 2012.

(25) Macrae, C. F.; Edgington, P. R.; McCabe, P.; Pidcock, E.; Shields, G. P.; Taylor, R.; Towler, M.; Van De Streek, J. Mercury: Visualization and Analysis of Crystal Structures. *J. Appl. Crystallogr.* **2006**, *39* (3), 453−457.

(26) Groom, C. R.; Bruno, I. J.; Lightfoot, M. P.; Ward, S. C. The Cambridge Structural Database. *Acta Crystallogr. Sect. B Struct. Sci. Cryst. Eng. Mater.* **2016**, *72* (2), 171−179.

(27) Jacobsen, A. C.; Nielsen, S.; Brandl, M.; Bauer-Brandl, A. Drug Permeability Profiling Using the Novel Permeapad® 96-Well Plate. *Pharm. Res.* **2020**, *37* (6), 93.

(28) Tzanova, M. M.; Randelov, E.; Stein, P. C.; Hiorth, M.; di Cagno, M. P. Towards a Better Mechanistic Comprehension of Drug Permeation and Absorption: Introducing the Diffusion-Partitioning Interplay. *Int. J. Pharm.* **2021**, *608*, No. 121116.

(29) Kim, S.; Chen, J.; Cheng, T.; Gindulyte, A.; He, J.; He, S.; Li, Q.; Shoemaker, B. A.; Thiessen, P. A.; Yu, B.; Zaslavsky, L.; Zhang, J.; Bolton, E. E. PubChem 2023 Update. *Nucleic Acids Res.* **2023**, *51* (D1), D1373−D1380.

(30) Van Eijck, B. P.; Kroon, J. Structure Predictions Allowing More than One Molecule in the Asymmetric Unit. *Acta Crystallogr. Sect. B Struct. Sci.* **2000**, *56* (3), 535−542.

(31) Steed, K. M.; Steed, J. W. Packing Problems: High Z' Crystal Structures and Their Relationship to Cocrystals, Inclusion Compounds, and Polymorphism. *Chem. Rev.* **2015**, *115* (8), 2895−2933.

(32) Elder, D. P.; Delaney, E.; Teasdale, A.; Eyley, S.; Reif, V. D.; Jacq, K.; Facchine, K. L.; Oestrich, R. S.; Sandra, P.; David, F. The Utility of Sulfonate Salts in Drug Development. *J. Pharm. Sci.* **2010**, *99* (7), 2948−2961.

(33) Hubatsch, I.; Ragnarsson, E. G. E.; Artursson, P. Determination of Drug Permeability and Prediction of Drug Absorption in Caco-2 Monolayers. *Nat. Protoc.* **2007**, *2* (9), 2111−2119.

(34) Gupta, R.; Dwadasi, B. S.; Rai, B.; Mitragotri, S. Effect of Chemical Permeation Enhancers on Skin Permeability: In Silico Screening Using Molecular Dynamics Simulations. *Sci. Rep.* **2019**, *9* (1), 1456 DOI: 10.1038/s41598-018-37900-0.

(35) Khatioda, R.; Saikia, B.; Das, P. J.; Sarma, B. Solubility and: In Vitro Drug Permeation Behavior of Ethenzamide Cocrystals Regulated in Physiological PH Environments. *CrystEngComm* **2017**, *19* (46), 6992−7000.

(36) Sanphui, P.; Devi, V. K.; Clara, D.; Malviya, N.; Ganguly, S.; Desiraju, G. R. Cocrystals of Hydrochlorothiazide: Solubility and Diffusion/Permeability Enhancements through Drug-Coformer Interactions. *Mol. Pharmaceutics* **2015**, *12* (5), 1615−1622.

https://doi.org/10.1021/acs.cgd.3c01488
Cryst. Growth Des. XXXX, XXX, XXX−XXX